energies

Article

Implementation of an Alternative Frequency-Dependent Three-Phase Transmission Line Model Based on the Folded Line Equivalent Model in MatLab-Simulink

Jaimis Sajid Leon Colqui [1,*], Luis Timaná [2], Pablo Torrez Caballero [1,3], José Pissolato Filho [1] and Sérgio Kurokawa [4]

[1] School of Electrical and Computer Engineering, State University of Campinas (UNICAMP), Campinas 13083-852, Brazil
[2] Department of Electronic and Telecommunications Engineering, Catholic University of Colombia, Bogotá 110231, Colombia
[3] Research and Development Center in Telecommunications (CPQD), Campinas 13086-902, Brazil
[4] Department of Electrical Engineering, São Paulo State University (UNESP), Ilha Solteira 15385-000, Brazil
* Correspondence: jeimis.leon@gmail.com

Abstract: This paper proposes an alternative multiconductor transmission line model that combines the folded line equivalent with the modal transformation. The folded line equivalent decomposes the nodal admittance matrix of a transmission line into its open-circuit and short-circuit contributions. These contributions are fitted to rational functions, which are associated with Norton equivalent circuits based on their state space models. The proposed model uses an orthogonal matrix to transform voltages and currents from the phase domain to the folded line equivalent domain and vice versa. Because the transformation matrix is orthogonal, we represent it using ideal transformers in simulation software. First, we use a circuit representation of Clarke's matrix to decompose a transmission line into its modes. Then, each mode is decomposed into its open-circuit and short-circuit contributions using a circuit implementation of the proposed matrix. The proposed approach can accurately represent short lines in simulations with time steps equal to or greater than the propagation time of the transmission line. We compare the results obtained with the proposed approach to those obtained with power systems computer-aided design/electromagnetic transients including the DC universal line model.

Keywords: transmission line modeling; Norton equivalent; folded line equivalent; electromagnetic transient

Citation: Leon Colqui, J.S.; Timaná L.; Caballero, P.T.; Pissolato Filho, J.; Kurokawa, S. Implementation of an Alternative Frequency-Dependent Three-Phase Transmission Line Model Based on the Folded Line Equivalent Model in MatLab-Simulink. *Energies* **2022**, *15*, 9302. https://doi.org/10.3390/en15249302

Academic Editors: Andrea Bonfiglio and Andrea Mazza

Received: 5 February 2022
Accepted: 9 March 2022
Published: 8 December 2022

1. Introduction and Literature Review

Frequency-dependent cable and transmission line (TL) models have been widely used in the study of electromagnetic transients in power systems. These models can be developed in the modal domain or directly in the phase domain. For instance, the JMarti model, introduced in [1], assumes a constant matrix to transform electrical parameters to the mode domain and vice versa. This assumption is valid for ideally transposed TLs and gives good results for non-transposed TLs with vertical symmetry. For this reason, the JMarti model is available as a built-in model in simulation software such as the Alternative Transient Program-Electromagnetic Transients Program (ATP-EMTP) [2]. However, assuming frequency-independent transformation matrices is not valid for non-transposed asymmetric lines or parallel circuits. Other TL models that do not make this assumption are preferred for these cases e.g., the universal line model (ULM) [3]. The ULM computes voltages and currents directly in the phase domain and is considered one of the most accurate and general models for the simulation of overhead transmission lines and cables. The ULM is available as a built-in model in simulation software such as the

Power Systems Computer Aided Design (PSCAD) [4] and the Electromagnetic Transients Program—Restructured Version (EMTP-RV) [5].

Numerous transmission line models (including the ULM and the JMarti model) derive from the method of characteristics. The method of characteristics requires (simulation) time steps to be smaller than the propagation time of the transmission line. Therefore, the time step used in the simulation of complex power systems is limited to the propagation time of the shortest line [6,7]. The folded line equivalent (FLE) [8] circumvents this problem. The FLE decouples a TL into two blocks that represent the short-circuit and open-circuit contributions of the TL. These blocks are fitted to rational functions using the vector fitting (VF) algorithm [9,10]. The state-space representations of the open-circuit and short-circuit contributions are then associated with equivalent Norton circuits, which are compatible with simulation software such as the EMTP. The main advantage of the FLE is that it provides accurate results for short lines when the time step is greater than the propagation time of the transmission line, reducing execution times in the simulation of complex power systems. In contrast, other transmission line models require smaller time steps and thereby take longer to compute simulations.

This paper proposes an EMTP-compatible multi-conductor TL model based on the FLE. The proposed model first transforms voltages and currents to the mode domain using a circuit representation of Clarke's matrix. Then, voltages and currents are transformed to the FLE domain using a new orthogonal transformation matrix, different from the one originally proposed in [8]. The proposed transformation matrix has a simpler interpretation and allows a more intuitive implementation using ideal transformers, similar to the arrangement used to represent Clarke's matrix. We implement the proposed model in the MatLab/Simulink simulation software [11].

The proposed approach inherits the advantages of the FLE and thus can be simulated with time steps greater than the propagation time of the TL. Because our approach is combined with modal transformation, it provides a better understanding of mode behavior during high-frequency phenomena such as lightning strikes or switching operations, which could cause outages and damage equipment. Moreover, analyzing three independent modes is simpler and computationally more efficient than analyzing a coupled three-phase TL. Because the proposed model uses basic circuit elements, it can be implemented in simulation software e.g., EMTP-RV, PSCAD/EMTDC, and ATP. Results show that the proposed approach outputs accurate results when the step size of the simulations is greater than the propagation time of the TL.

2. The Folded Line Equivalent

The nodal admittance matrix of the TL of Figure 1 relates voltages $\boldsymbol{V}_1 = \begin{bmatrix} V_{1,1} & \dots & V_{n,1} \end{bmatrix}^T$ and currents $\boldsymbol{I}_1 = \begin{bmatrix} I_{1,1} & \dots & I_{2,1} \end{bmatrix}^T$ at one of the line terminals to the voltages $\boldsymbol{V}_2 = \begin{bmatrix} V_{1,2} & \dots & V_{n,2} \end{bmatrix}^T$ and currents $\boldsymbol{I}_2 = \begin{bmatrix} I_{1,2} & \dots & I_{2,2} \end{bmatrix}^T$ at the other terminal, as follows:

$$\begin{bmatrix} \boldsymbol{I}_1 \\ \boldsymbol{I}_2 \end{bmatrix} = \begin{bmatrix} \boldsymbol{Y}_s & \boldsymbol{Y}_m \\ \boldsymbol{Y}_m & \boldsymbol{Y}_s \end{bmatrix} \begin{bmatrix} \boldsymbol{V}_1 \\ \boldsymbol{V}_2 \end{bmatrix}. \quad (1)$$

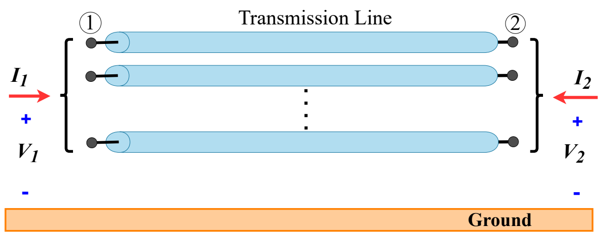

Figure 1. Multiconductor transmission line.

Refs. [12–14] compute the frequency-dependent nodal admittance matrix in (1) from the per unit length (p.u.l.) TL parameters. The FLE takes advantage of the symmetry of the nodal admittance matrix in (1) and decouples it into its open-circuit and short-circuit contributions as follows:

$$\begin{bmatrix} \boldsymbol{I}_{\text{oc}} \\ \boldsymbol{I}_{\text{sc}} \end{bmatrix} = \begin{bmatrix} \boldsymbol{Y}_{\text{oc}} & \mathbf{0} \\ \mathbf{0} & \boldsymbol{Y}_{\text{sc}} \end{bmatrix} \begin{bmatrix} \boldsymbol{V}_{\text{oc}} \\ \boldsymbol{V}_{\text{sc}} \end{bmatrix} \tag{2}$$

where the open-circuit admittance $\boldsymbol{Y}_{\text{oc}}$ and the short-circuit admittance $\boldsymbol{Y}_{\text{sc}}$ are, respectively, given by

$$\boldsymbol{Y}_{\text{oc}} = \boldsymbol{Y}_{\text{s}} + \boldsymbol{Y}_{\text{m}} \tag{3}$$

$$\boldsymbol{Y}_{\text{sc}} = \boldsymbol{Y}_{\text{s}} - \boldsymbol{Y}_{\text{m}}. \tag{4}$$

Voltages and currents are transformed to and from the FLE domain as follows:

$$\begin{bmatrix} \boldsymbol{V}_{\text{oc}} \\ \boldsymbol{V}_{\text{sc}} \end{bmatrix} = \boldsymbol{K}^{-1} \begin{bmatrix} \boldsymbol{V}_1 \\ \boldsymbol{V}_2 \end{bmatrix} \tag{5}$$

$$\begin{bmatrix} \boldsymbol{I}_{\text{oc}} \\ \boldsymbol{I}_{\text{sc}} \end{bmatrix} = \boldsymbol{K}^{-1} \begin{bmatrix} \boldsymbol{I}_1 \\ \boldsymbol{I}_2 \end{bmatrix} \tag{6}$$

where the transformation matrix $\boldsymbol{K}^{-1}$ is given by

$$\boldsymbol{K} = \begin{bmatrix} \mathbf{U} & \mathbf{U} \\ \mathbf{U} & -\mathbf{U} \end{bmatrix}, \tag{7}$$

and $\mathbf{U}$ is the identity matrix.

3. Our Approach: Proposed Folded Line Equivalent

The transformation of voltages $\boldsymbol{V}$ and currents $\boldsymbol{I}$ at line terminals, longitudinal impedances $\boldsymbol{Z}$, and shunt admittances $\boldsymbol{Y}$ of the TL of Figure 1 from the phase domain to the mode domain and vice versa is given by

$$\boldsymbol{V} = \boldsymbol{T}_{\text{V}}\, \boldsymbol{V}_{\alpha\beta 0} \tag{8}$$

$$\boldsymbol{I} = \boldsymbol{T}_{\text{I}}\, \boldsymbol{I}_{\alpha\beta 0} \tag{9}$$

$$\boldsymbol{Z}_{\alpha\beta 0} = \boldsymbol{T}_{\text{I}}^{\text{T}} \boldsymbol{Z} \boldsymbol{T}_{\text{I}} \tag{10}$$

$$\boldsymbol{Y}_{\alpha\beta 0} = \boldsymbol{T}_{\text{I}}^{-1} \boldsymbol{Y} \boldsymbol{T}_{\text{I}}^{-\text{T}}. \tag{11}$$

In (8) and (9), the transformation matrices $\boldsymbol{T}_{\text{I}}$ and $\boldsymbol{T}_{\text{V}}$ are frequency-dependent.

Clarke's matrix (12) is a frequency-constant orthogonal transformation matrix that gives accurate results for perfectly transposed TLs and relatively accurate results for TLs with vertical symmetry [15].

$$\boldsymbol{T}_{\text{clk}} = \begin{bmatrix} 2/\sqrt{6} & -1/\sqrt{6} & -1/\sqrt{6} \\ 0 & 1/\sqrt{2} & -1/\sqrt{2} \\ 1/\sqrt{3} & 1/\sqrt{3} & 1/\sqrt{3} \end{bmatrix} \tag{12}$$

We propose to use Clarke's matrix to decouple three-phase TLs into its modes, as shown in Figure 2. Then, we transform each independent mode to the FLE domain, as shown in Figure 3. We represent each of these transformations using circuit elements, as shown in Figure 4.

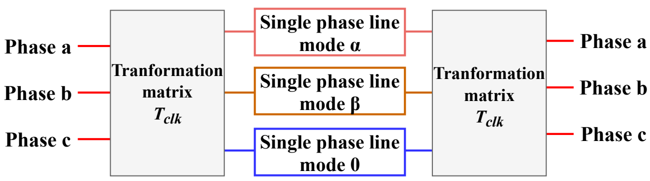

Figure 2. Representation of a three-phase transmission line in the mode domain: abc ⇔ $\alpha\beta 0$ ⇔ abc.

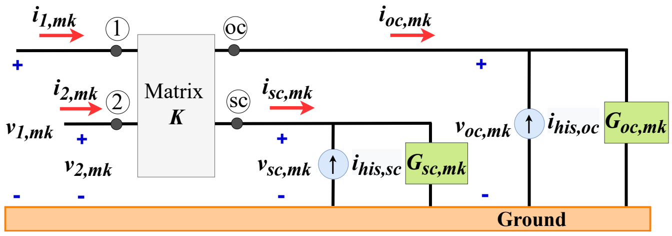

Figure 3. Mode representation for the proposed FLE (PFLE) model.

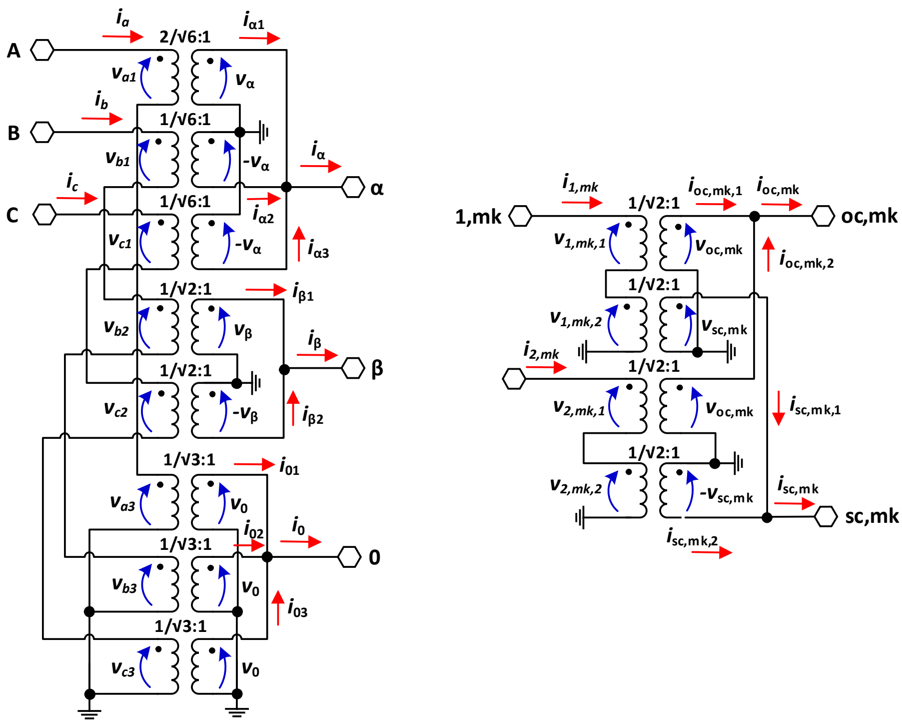

(**a**) (**b**)

Figure 4. Circuit representation of (**a**) Clarke's matrix ($\alpha\beta0$ transformation) and (**b**) the proposed FLE transformation matrix (FLE transformation).

3.1. Modal Transformation: Circuit Representation of Clarke's Matrix

The block labeled as *transformation matrix* in Figure 2 transforms voltages and currents from the phase domain to the mode domain and vice versa. This block contains the arrangement of ideal transformers of Figure 4a [16], which relates voltages at the left and right terminals Figure 4a as follows:

$$v_a = v_{a1} + v_{a3} = \frac{2}{\sqrt{6}}v_\alpha + \frac{1}{\sqrt{3}}v_0 \tag{13}$$

$$v_b = v_{b1} + v_{b2} + v_{b3} = -\frac{1}{\sqrt{6}}v_\alpha + \frac{1}{\sqrt{2}}v_\beta + \frac{1}{\sqrt{3}}v_0 \tag{14}$$

$$v_c = v_{c1} + v_{c2} + v_{c3} = -\frac{1}{\sqrt{6}}v_\alpha + \frac{1}{\sqrt{2}}v_\beta + \frac{1}{\sqrt{3}}v_0 \tag{15}$$

The relationship between currents at right and left terminals of Figure 4a is given by

$$i_\alpha = i_{\alpha1} + i_{\alpha2} + i_{\alpha3} = \frac{2}{\sqrt{6}}i_a - \frac{1}{\sqrt{6}}i_b - \frac{1}{\sqrt{6}}i_c \tag{16}$$

$$i_\beta = i_{\beta2} + i_{\beta3} = \frac{1}{\sqrt{2}}i_b - \frac{1}{\sqrt{2}}i_c \tag{17}$$

$$i_0 = i_{01} + i_{02} + i_{03} = \frac{1}{\sqrt{3}}i_{\mathrm{a}} + \frac{1}{\sqrt{3}}i_{\mathrm{b}} + \frac{1}{\sqrt{3}}i_{\mathrm{c}} \tag{18}$$

In matrix form, the relationships presented in (13)–(18) can be written as follows:

$$\boldsymbol{V}_{\mathrm{abc}} = \boldsymbol{T}_{\mathrm{clk}}^{-1}\boldsymbol{V}_{\alpha\beta 0} \tag{19}$$

$$\boldsymbol{I}_{\alpha\beta 0} = \boldsymbol{T}_{\mathrm{clk}}\boldsymbol{V}_{abc} \tag{20}$$

which is equivalent to (9) when $\boldsymbol{T}_{\mathrm{I}} = \boldsymbol{T}_{\mathrm{clk}}$ (Clarke's transformation).

3.2. FLE Transformation: Circuit Representation of the Proposed Transformation Matrix

We combine the circuit representation of the $\alpha\beta 0$ decomposition of Section 3.1 with the circuit representation of the FLE transformation presented in this section. After the three-phase TL is decomposed into its modes, as shown in Figure 2, each mode is individually transformed to the FLE domain, as shown in Figure 3. Each mode has its open-circuit (OC) and short-circuit (SC) contributions. The block labeled as *Matrix K* in Figure 3 transforms voltages and currents from the mode domain to the FLE domain and vice versa. This block contains the arrangement of ideal transformers of Figure 4b, which relates voltages at terminals 1 and 2 to voltages at terminals OC and SC as follows:

$$V_{1,\mathrm{mk}} = V_{1,\mathrm{mk1}} + V_{1,\mathrm{mk2}} = \frac{1}{\sqrt{2}}V_{\mathrm{oc,mk}} + \frac{1}{\sqrt{2}}V_{\mathrm{sc,mk}} \tag{21}$$

$$V_{2,\mathrm{mk}} = V_{2,\mathrm{mk1}} + V_{2,\mathrm{mk2}} = \frac{1}{\sqrt{2}}V_{\mathrm{oc,mk}} - \frac{1}{\sqrt{2}}V_{\mathrm{sc,mk}} \tag{22}$$

where subscript mk = $\{\alpha, \beta, 0\}$. The relationship between currents at terminals 1 and 2 to voltages at terminals OC and SC is given by

$$I_{\mathrm{oc,mk}} = I_{\mathrm{oc,mk1}} + I_{\mathrm{oc,mk2}} = \frac{1}{\sqrt{2}}I_{1,\mathrm{mk}} + \frac{1}{\sqrt{2}}I_{2,\mathrm{mk}} \tag{23}$$

$$I_{\mathrm{sc,mk}} = I_{\mathrm{sc,mk1}} + I_{\mathrm{sc,mk2}} = \frac{1}{\sqrt{2}}I_{1,\mathrm{mk}} - \frac{1}{\sqrt{2}}I_{2,\mathrm{mk}} \tag{24}$$

In matrix form, the relationships presented in (21)–(24) can be written as follows:

$$\begin{bmatrix} V_{1,\mathrm{mk}} \\ V_{2,\mathrm{mk}} \end{bmatrix} = \boldsymbol{K}\begin{bmatrix} V_{\mathrm{oc,mk}} \\ V_{\mathrm{sc,mk}} \end{bmatrix} \tag{25}$$

$$\begin{bmatrix} I_{\mathrm{oc,mk}} \\ I_{\mathrm{sc,mk}} \end{bmatrix} = \boldsymbol{K}^{-1}\begin{bmatrix} I_{1,\mathrm{mk}} \\ I_{2,\mathrm{mk}} \end{bmatrix}. \tag{26}$$

In (25) and (26), instead of using the transformation *Matrix K* introduced in [8], we propose using the following transformation matrix to decouple single-phase TL into its open-circuit and short-circuit contributions.

$$\boldsymbol{K} = \begin{bmatrix} \frac{1}{\sqrt{2}} & \frac{1}{\sqrt{2}} \\ \frac{1}{\sqrt{2}} & -\frac{1}{\sqrt{2}} \end{bmatrix} \tag{27}$$

The proposed transformation matrix preserves the properties and relationships of the transformation matrix introduced in [8], yet it allows a simpler and more intuitive implementation. Figure 4b shows the circuit implementation of (27) using an arrangement of ideal transformers.

3.3. Computation of the Nodal Admittance Matrix of Each Mode

Each of the modes resulting from the transformation presented in Section 3.1 is considered an independent transmission line and thus has a nodal admittance matrix given by

$$\boldsymbol{Y}_{\mathrm{mk}} = \begin{bmatrix} Y_{\mathrm{mk,s}} & Y_{\mathrm{mk,m}} \\ Y_{\mathrm{mk,m}} & Y_{\mathrm{mk,s}} \end{bmatrix}. \tag{28}$$

The nodal admittance matrix of the mk-th mode can be calculated from the propagation function H_{mk} and characteristic admittance $Y_{\mathrm{c,mk}}$ of the mode as follows

$$Y_{\mathrm{mk,s}} = \left(1 - H_{\mathrm{mk}}^2\right)^{-1}\left(H_{\mathrm{mk}}^2 + 1\right)Y_{\mathrm{c,mk}} \tag{29}$$

$$Y_{\mathrm{mk,m}} = -2\left(1 - H_{\mathrm{mk}}^2\right)^{-1}H_{\mathrm{mk}}Y_{\mathrm{c,mk}} \tag{30}$$

where H_{mk} and $Y_{\mathrm{c,mk}}$ are computed from the mode's p.u.l. impedance Z_{mk}, p.u.l. admittance Y_{mk}, and the length of the line ℓ, as shown below

$$Y_{\mathrm{c,k}} = Z_{\mathrm{mk}}^{-1}\sqrt{Z_{\mathrm{mk}}Y_{\mathrm{mk}}} \tag{31}$$

$$H_{\mathrm{k}} = \mathrm{e}^{-\ell\sqrt{Y_{\mathrm{mk}}Z_{\mathrm{mk}}}}. \tag{32}$$

There are alternative procedures of computing $Y_{\mathrm{mk,s}}$ and $Y_{\mathrm{mk,m}}$. In [12], Morched et al. compute the elements of the modal admittance matrix of a single-phase TL as follows:

$$Y_{\mathrm{mk,s}} = Y_{\mathrm{mk}}\Lambda_{\mathrm{mk,zy}}^{-1}\coth\left(\Lambda_{\mathrm{mk,zy}}\ell\right) \tag{33}$$

$$Y_{\mathrm{k,m}} = -Y_{\mathrm{mk}}\Lambda_{\mathrm{mk,zy}}^{-1}\mathrm{csch}\left(\Lambda_{\mathrm{mk,zy}}\ell\right) \tag{34}$$

where propagation constant $\Lambda_{\mathrm{mk,zy}} = \sqrt{Z_{\mathrm{mk}}Y_{\mathrm{mk}}}$. Alternatively, in [14], Gustavsen avoids hyperbolic functions and computes $Y_{\mathrm{mk,s}}$ and $Y_{\mathrm{mk,m}}$ as follows:

$$Y_{\mathrm{mk,s}} = Z_{\mathrm{mk}}^{-1}a_{\mathrm{mk}} \tag{35}$$

$$Y_{\mathrm{mk,m}} = Z_{\mathrm{mk}}^{-1}b_{\mathrm{mk}} \tag{36}$$

where

$$a_{\mathrm{mk}} = \frac{\sqrt{d_{\mathrm{mk}}}\left(1 + h_{\mathrm{mk}}^2\right)}{1 - h_{\mathrm{mk}}^2} \tag{37}$$

$$b_{\mathrm{mk}} = \frac{-2\sqrt{d_{\mathrm{mk}}}.h_{\mathrm{mk}}}{1 - h_{\mathrm{mk}}^2} \tag{38}$$

$$h_{\mathrm{mk}} = \exp\left(-\sqrt{d_{\mathrm{mk}}}\ell\right) \tag{39}$$

$$d_{\mathrm{mk}} = \left(\sqrt{Z_{\mathrm{mk}}Y_{\mathrm{mk}}}\right)^{-1} \tag{40}$$

3.4. Circuit Representation of the FLE Parameters of Each Mode

The FLE parameters (open-circuit and short-circuit contributions) of each mode can be represented by Norton equivalent circuits [17] or an arrangement of resistors, capacitors, and inductors [18]. In this paper, we employ Norton equivalent circuits to represent the open-circuit and short-circuit contributions for each mode in simulation software.

The VF algorithm [9,10] fits the open-circuit $Y_{\mathrm{oc,mk}}$ and short-circuit $Y_{\mathrm{sc,mk}}$ contributions of each mode to rational functions. We use both the VF algorithm and the fast modal perturbation (FMP) [19] to ensure passivity in the fitted rational functions. The state-space model of each fitted matrix is then generated following the procedure described in [20]. The state-space model that describes the open-circuit contribution of the mk-th mode is given by

$$\dot{\boldsymbol{x}}_{\mathrm{mk,oc}}(t) = \boldsymbol{A}_{\mathrm{mk,oc}}\boldsymbol{x}_{\mathrm{mk,oc}}(t) + \boldsymbol{B}_{\mathrm{mk,oc}}v_{\mathrm{mk,oc}}(t) \tag{41}$$

$$i_{\mathrm{mk,oc}}(t) = \boldsymbol{C}_{\mathrm{mk,oc}}\boldsymbol{x}_{\mathrm{mk,oc}}(t) + D_{\mathrm{mk,oc}}v_{\mathrm{mk,oc}}(t) \tag{42}$$

Similarly, the state-space model that describes the short-circuit contribution of the mk-th mode is given by

$$\dot{\boldsymbol{x}}_{\mathrm{mk,sc}}(t) = \boldsymbol{A}_{\mathrm{mk,sc}}\boldsymbol{x}_{\mathrm{mk,sc}}(t) + \boldsymbol{B}_{\mathrm{mk,sc}}\boldsymbol{v}_{\mathrm{mk,sc}}(t) \tag{43}$$

$$i_{\mathrm{mk,sc}}(t) = \boldsymbol{C}_{\mathrm{mk,sc}}\boldsymbol{x}_{\mathrm{mk,sc}}(t) + D_{\mathrm{mk,sc}}v_{\mathrm{mk,sc}}(t) \tag{44}$$

In (41)–(44), state matrices $\boldsymbol{A}$, $\boldsymbol{B}$, $\boldsymbol{C}$, and D are constant.

The Norton equivalent circuit of a state-space model consists of a constant conductance G and a historic current i_{hist} that updates its value in each time step, as portrayed in Figure 3. The historic current sources and the constant parameters of the Norton equivalent circuit allow the proposed model to consider the wave phenomena. Application of the trapezoidal rule of integration to (41)–(44) results in the following Norton parameters [17]:

$$G_{\mathrm{ck,mk}} = D_{\mathrm{ck,mk}} + \boldsymbol{C}_{\mathrm{ck,mk}}\boldsymbol{\lambda}_{\mathrm{ck,mk}}\boldsymbol{B}_{\mathrm{ck,mk}} \tag{45}$$

$$i_{\mathrm{hist,ck,mk}}[n] = -\boldsymbol{C}_{\mathrm{ck,mk}}(\boldsymbol{\alpha}_{\mathrm{ck,mk}} + 1)\boldsymbol{\lambda}_{\mathrm{ck,mk}}\boldsymbol{x}_{\mathrm{ck,mk}}[n] \tag{46}$$

where

$$\boldsymbol{\lambda}_{\mathrm{ck,mk}} = \left(1 - \boldsymbol{A}_{\mathrm{ck,mk}}\frac{\Delta t}{2}\right)^{-1}\frac{\Delta t}{2} \tag{47}$$

$$\boldsymbol{\alpha}_{\mathrm{ck,mk}} = \left(1 - \boldsymbol{A}_{\mathrm{ck,mk}}\frac{\Delta t}{2}\right)^{-1}\left(1 + \boldsymbol{A}_{\mathrm{ck,mk}}\frac{\Delta t}{2}\right) \tag{48}$$

$$\boldsymbol{x}_{\mathrm{ck,mk}}[n] = \boldsymbol{\alpha}_{\mathrm{ck,mk}}\boldsymbol{x}_{\mathrm{ck,mk}}[n-1] + \boldsymbol{B}_{\mathrm{ck,mk}}v_{\mathrm{ck,mk}}[n-1] \tag{49}$$

and ck = $\{$oc,sc$\}$, mk = $\{\alpha, \beta, 0\}$. The Norton parameters in (45) and (46) are EMTP-compatible because all passive components are represented by Norton equivalent circuits [6].

4. Results

4.1. Line Configuration and Simulation Approach

To show results, we

- Computed the p.u.l. line parameters of the TL of Figure 5 using the PSCAD/EMTDC's Line Constants Program;
- Simulated the TL using the proposed approach, implemented in Matlab/Simulink, as shown in Figure 4;
- Simulated the TL using PSCAD/EMTDC's ULM;
- Compared the outputs of both models.

The flowchart of Figure 6 shows all the steps mentioned above, needed to implement the proposed model in MatLab's Simulink (ver. 2021b).

One of the benefits of the proposed approach is that it provides accurate results when the time step is greater than the propagation delay of the TL. This is particularly useful in networks containing short and long lines because the time step of the entire network depends on the propagation delay of the shortest line. To show this advantage, we considered the TL of Figure 5 300 m long, resulting in a propagation delay of approximately 1 µs. We show that the PFLE outputs accurate results in simulations with time steps greater than 1 µs.

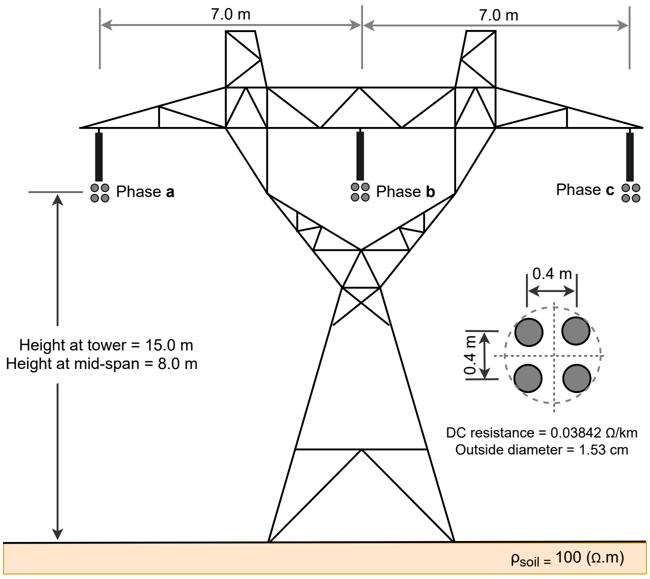

Figure 5. Three-phase transmission line geometry.

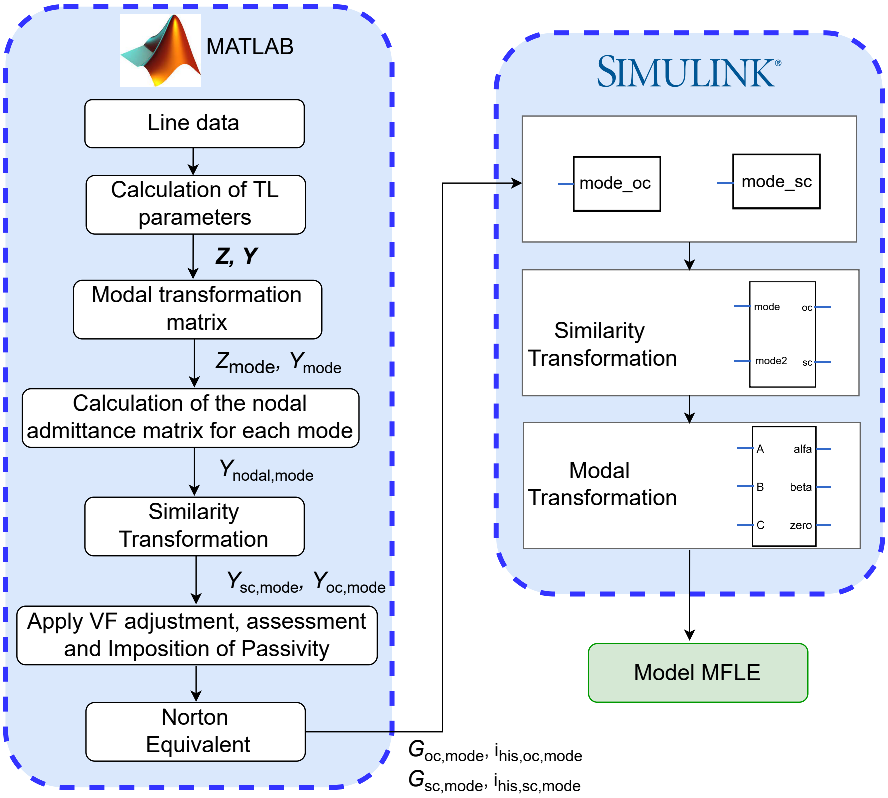

Figure 6. Steps required to implement the PFLE in MatLab's Simulink.

4.2. Fitting Procedure and Passivity Enforcement

The TL of Figure 5 has three modes of propagation: α, β, and 0. Each mode is composed of an open-circuit and short-circuit nodal admittance.

We employed the VF routine [21] to fit the open-circuit and short-circuit admittances of each mode using twenty poles and five iterations. Passivity is independently enforced for each mode using the "*RPdriver*" routine [20]. Note that the "*RPdriver*" routine is applied to a frequency range that is twice the fitting frequency. Therefore, it is necessary to compute parameters up to 2 MHz.

Figures 7–9 show the magnitude of the open-circuit and short-circuit nodal admittance of each mode (solid blue line), the fitted rational function after enforcing passivity (dotted red line), and the deviation between them (solid green line). Note that the deviation curve has a behavior similar to the data because the weight used in the fitting is inversely proportional to the magnitude of the data. This weighting scheme allows the accurate fitting of small and large values.

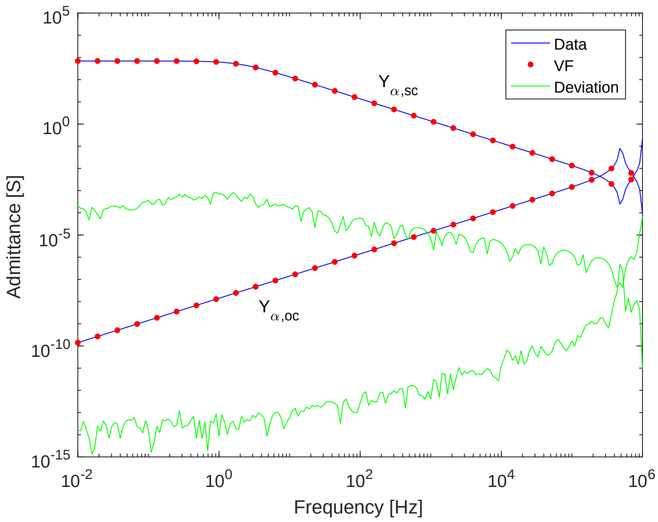

Figure 7. Fitting of the open-circuit admittance Y_{oc} and short-circuit admittance Y_{sc} of mode α.

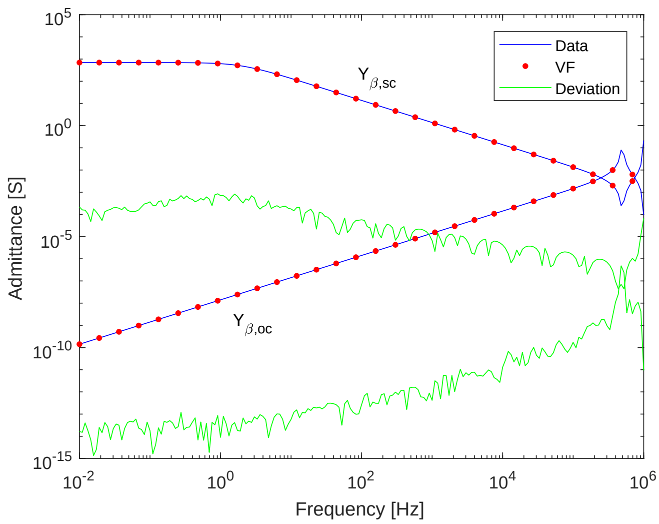

Figure 8. Fitting of the open-circuit admittance Y_{oc} and short-circuit admittance Y_{sc} of mode β.

The number of poles required to fit a given function usually depends on the number of peaks present in the curve. The number of peaks in the frequency range of power systems transients increases with the length of the line. As a result, short lines require fewer poles to achieve a certain level of accuracy. This paper shows that the proposed model outputs accurate results in the simulation of short lines even when the time step of the simulation is larger than the propagation delay of the TL.

A Norton equivalent circuit is considered passive when the eigenvalues of the real part of the open-circuit nodal admittance $Y_{oc,mk}$ and short-circuit nodal admittance $Y_{sc,mk}$ are positive for all frequencies [8,22].

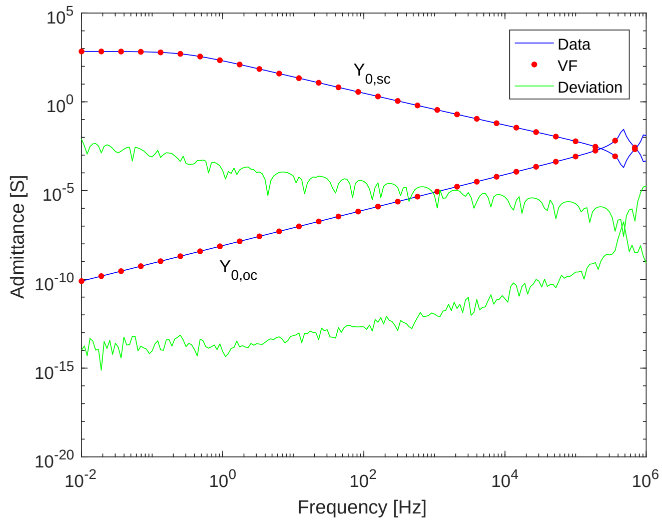

Figure 9. Fitting of the open-circuit admittance Y_{oc} and short-circuit admittance Y_{sc} of mode 0.

Figures 10–12 show that the eigenvalues of the open-circuit and short-circuit conductances of each mode are positive after passivity is enforced.

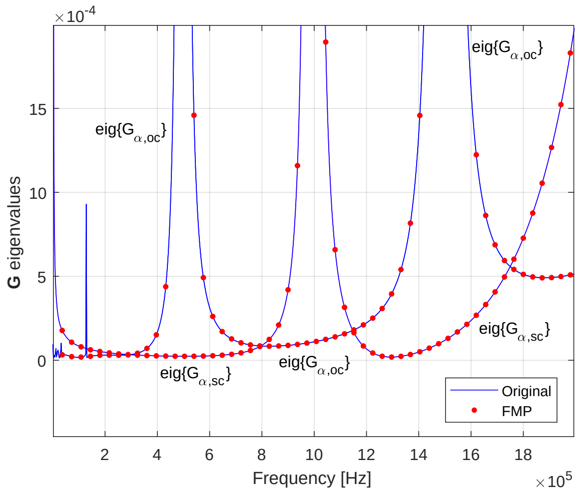

Figure 10. Eigenvalues of the nodal admittance matrix of mode α.

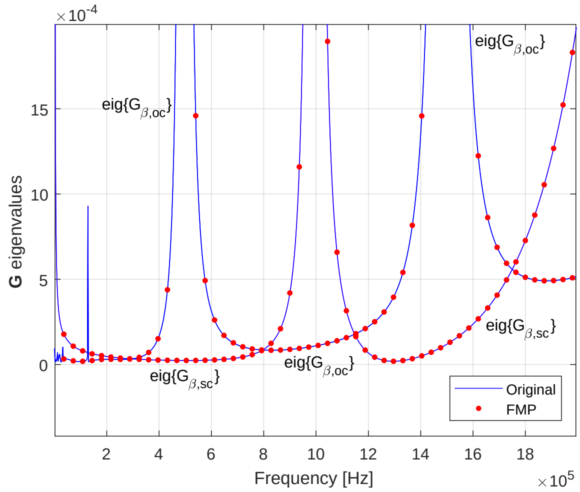

Figure 11. Eigenvalues of the nodal admittance matrix of mode β.

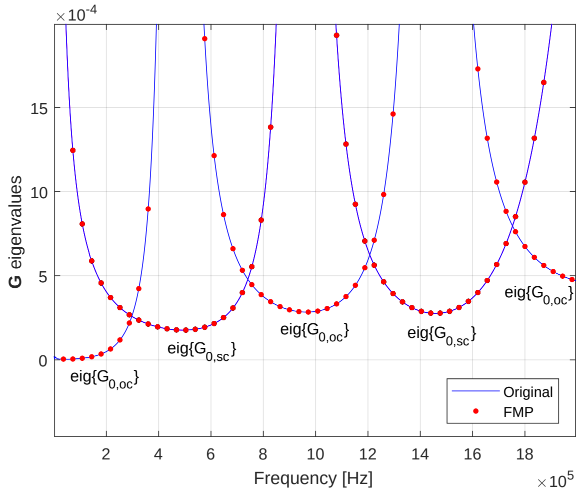

Figure 12. Eigenvalues of the nodal admittance matrix of mode 0.

4.3. Open-Circuit, Capacitive Load, and Single-Phase Fault

4.3.1. Simulation Layout

Figure 13 shows the TL of Figure 5 when one of its terminals is energized at 0 s, and the other terminal is

1. Left open-circuited when the line is energized;
2. Connected to a capacitive load at 4 ms;
3. A single-phase fault occurs at 8 ms.

We compared the results obtained by the proposed approach (labeled as PFLE) to those obtained by PSCAD's ULM. To show the advantages of the proposed approach, the simulations were performed considering different time steps.

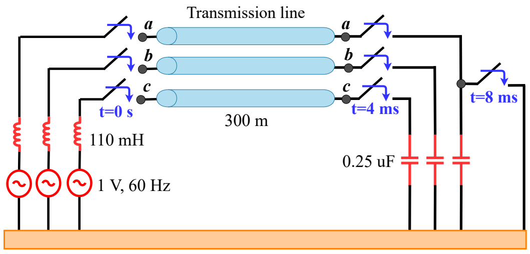

Figure 13. Simulation configuration.

4.3.2. Results

Results show that the proposed approach outputs accurate results even when the time step is four times the propagation delay of the TL. In contrast, the maximum integration time step that the ULM supports is equal to the propagation delay of the TL, which is approximately 1 µs. This requirement must be met for all line models based on the method of characteristics. We use a time step equal to 1/10 of the propagation delay of the TL to compute results using the ULM.

In all simulations, the red, blue, and green curves represent phases A, B, and C, respectively. The results are organized as follows:

1. Figures 14 and 15 show, respectively, the voltages at the receiving terminal and the currents at the sending terminal during line energization;
2. Figures 16 and 17 show, respectively, the voltages at the receiving terminal and the currents at the sending terminal when the capacitive load is connected;
3. Figures 18 and 19 show, respectively, the voltages at the receiving terminal and the currents at the sending terminal when a single-phase fault occurs at 8 ms.

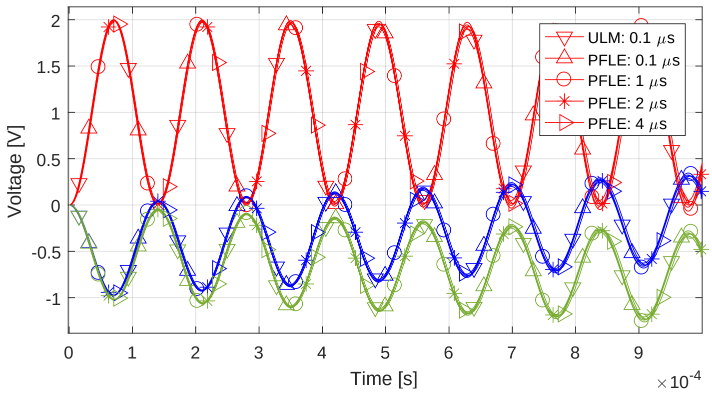

Figure 14. Voltage at the receiving end of the line when the line is energized.

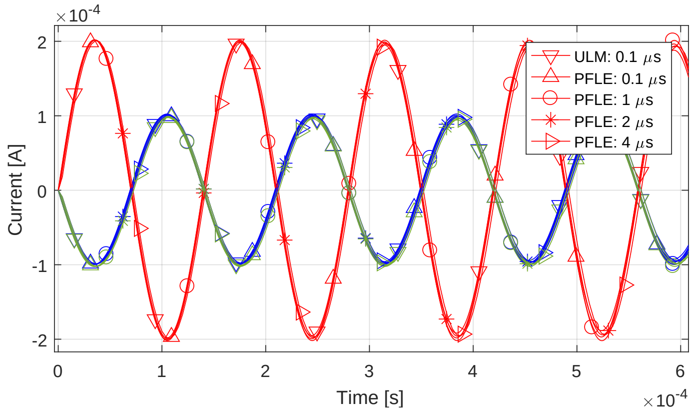

Figure 15. Current at the sending end of the line when the line is energized.

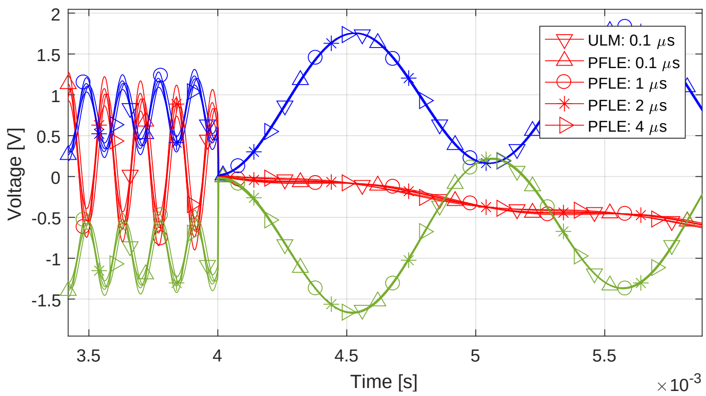

Figure 16. Voltage at the receiving end of the line when the cable is connected.

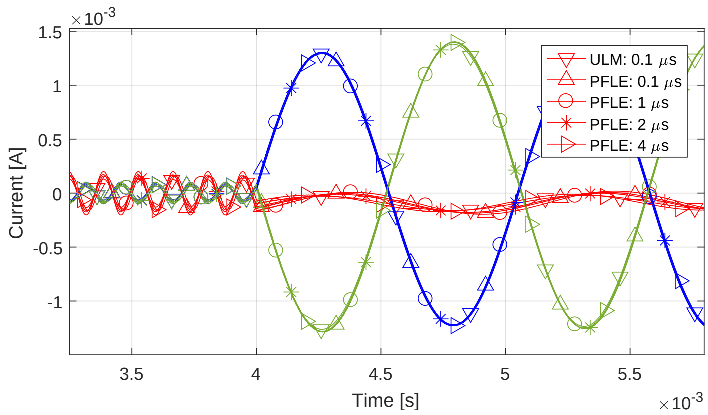

Figure 17. Current at the sending end of the line when the cable is connected.

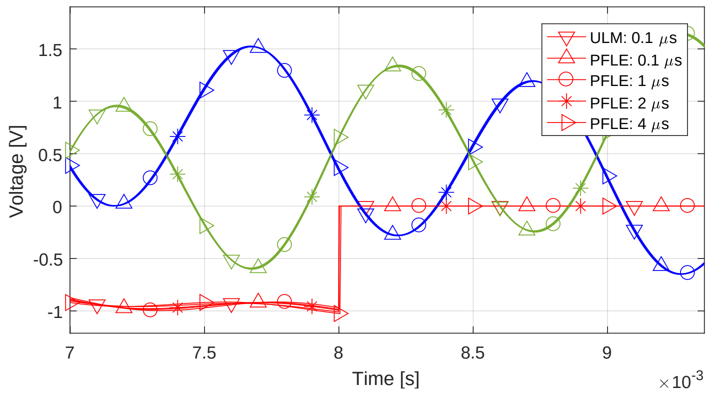

Figure 18. Voltage at the receiving end of the line after a single-phase fault occurs.

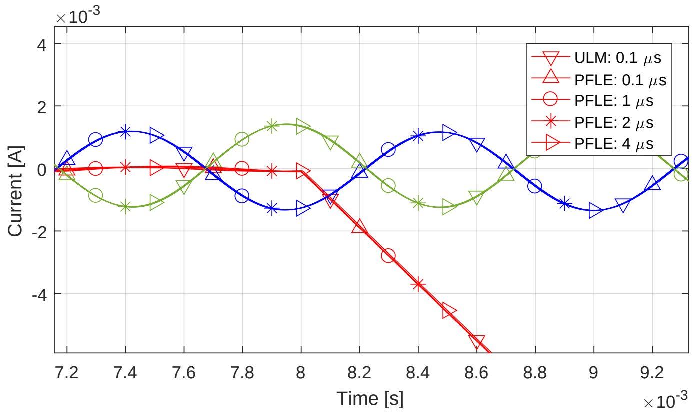

Figure 19. Current at the sending end of the line after a single-phase fault occurs.

Figures 14–19 show that the PFLE outputs accurate results with time steps greater than the propagation delay of the TL. This can greatly reduce execution times in the simulation of large complex networks where the time step is limited to the propagation delay of the shortest line when TL models based on the methods of characteristics are used.

4.4. Line Energization

4.4.1. Simulation Layout

Figure 20 shows the TL of Figure 5 when one of its terminals is energized at 0 s and the other terminal is connected to a resistive-inductive load.

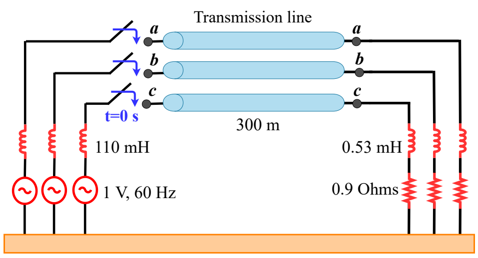

Figure 20. Transmission line connected to a resistive-inductive load.

4.4.2. Results

Figures 21 and 22 compare the voltages at the receiving terminal simulated with the proposed approach (labeled as PFLE) and PSCAD's ULM for several time steps. Figure 21 shows the transient voltages right after the line is energized, and Figure 22 shows the voltages after the first high-frequency voltages disappear. Note that using a time step greater than the propagation delay of the TL causes a small delay during the first high-frequency oscillations, which disappears as the TL reaches steady-state conditions, as shown in Figure 22.

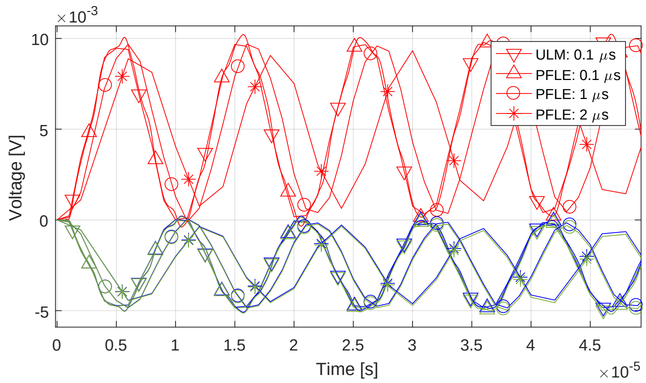

Figure 21. Voltages at the receiving terminal of the line right after it is energized.

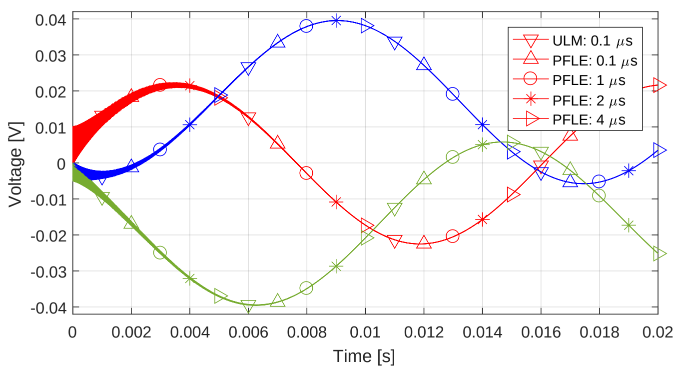

Figure 22. Voltages at the receiving end of the line in the first 20 ms of the simulation.

Figure 23 shows the currents at the sending terminal of the TL. Note that the proposed approach agrees with the ULM for all time steps.

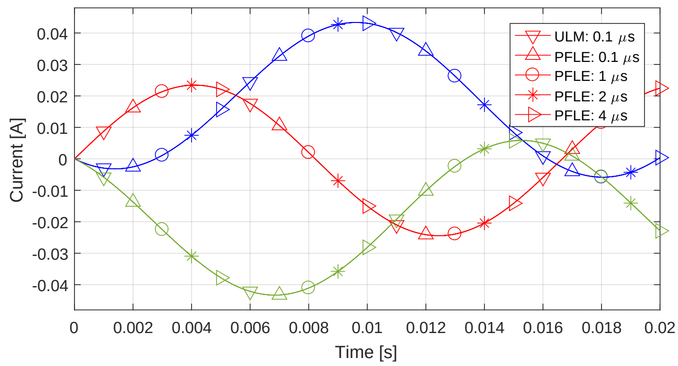

Figure 23. Current at the sending terminal of the line.

The execution time of a simulation depends on the time required to solve a single time step and the total number of time steps in the simulation. Reducing the average time to solve one time step is possible through optimization techniques and lightweight models. However, the most effective way of reducing the execution time of simulation is by reducing the total number of time steps that need to be computed. TL models based on the method of characteristics are limited to time steps equal to the propagation delay of the shortest TL in the network. The proposed approach supports time steps greater than the propagation delay of the shortest TL without compromising accuracy. Our results show that the proposed approach outputs accurate results even with time steps that are four times the propagation delay of the shortest TL, resulting in execution times that are up to 400% faster.

4.5. Error

Sections 4.3.2 and 4.4.2 show the results obtained by implementing the proposed approach, the PFLE, in MatLab's Simulink. We measure the error of the PFLE using the normalized root-mean-square deviation (NRMSD), which is given by

$$\mathrm{NRMSD} = \frac{\sqrt{\frac{1}{N}\sum_{i=1}^{N}\left(y_{PM,i} - y_{\mathrm{ULM}}\right)^2}}{\max\{y_{\mathrm{ULM}}\} - \min\{y_{\mathrm{ULM}}\}} \tag{50}$$

where N is the number of points of y.

In all simulations, we compare the results obtained by the PFLE to the results obtained by the ULM when the time step is 1/10 of the propagation delay of the TL (1 µs). We use PSCAD/EMTDC's ULM as a reference model because this model is widely accepted in technical literature and professional software due to its accuracy and numerical stability. The ULM computes results directly in the phase domain and time domain while considering the frequency dependence and distributed nature of line parameters.

Our numerical comparisons are organized as follows:

- Table 1 shows the NRMSD of the proposed approach (PFLE) in Figures 14 and 15.
- Table 2 shows the NRMSD of the proposed approach (PFLE) in Figures 16 and 17.
- Table 3 shows the NRMSDof the proposed approach (PFLE) in Figures 18 and 19.
- Table 4 shows the NRMSD of the proposed approach (PFLE) in Figures 22 and 23.

Table 1. NRMSD of the voltage and current curves obtained with the PFLE with respect to the voltage and current curves obtained with the ULM and a time step of 1 µs: Figures 14 and 15.

Voltage			Current		
Phases	**Model: Δt**	**NRMSD**	**Phases**	**Model: Δt**	**NRMSD**
1 (Figure 14)	PFLE: 0.1 µs	0.004	1 (Figure 15)	PFLE: 0.1 µs	1×10^{-4}
	PFLE: 1 µs	0.003		PFLE: 1 µs	3×10^{-4}
	PFLE: 2 µs	0.003		PFLE: 2 µs	1×10^{-4}
	PFLE: 4 µs	0.005		PFLE: 4 µs	2×10^{-4}
2 and 3 (Figure 14)	PFLE: 0.1 µs	0.005	2 and 3 (Figure 15)	PFLE: 0.1 µs	1×10^{-4}
	PFLE: 1 µs	0.003		PFLE: 1 µs	2×10^{-4}
	PFLE: 2 µs	0.003		PFLE: 2 µs	4×10^{-4}
	PFLE: 4 µs	0.005		PFLE: 4 µs	1×10^{-4}

Table 2. NRMSD of the voltage and current curves obtained with the PFLE with respect to the voltage and current curves obtained with the ULM and a time step of 1 µs: Figures 16 and 17.

Voltage			Current		
Phases	**Model: Δt**	**NRMSD**	**Phases**	**Model: Δt**	**NRMSD**
1 (Figure 16)	PFLE 0.1 µs	0.004	1 (Figure 17)	PFLE 0.1 µs	2×10^{-4}
	PFLE 1 µs	0.003		PFLE 1 µs	3×10^{-4}
	PFLE 2 µs	0.003		PFLE 2 µs	4×10^{-4}
	PFLE 4 µs	0.005		PFLE 4 µs	1×10^{-4}
2 and 3 (Figure 16)	2	0.005	2 and 3 (Figure 17)	PFLE 0.1 µs	2×10^{-4}
	PFLE 1 µs	0.003		PFLE 1 µs	1×10^{-4}
	PFLE 2 µs	0.003		PFLE 2 µs	2×10^{-4}
	PFLE 4 µs	0.005		PFLE 4 µs	3×10^{-4}

Table 3. NRMSD of the voltage and current curves obtained with the PFLE with respect to the voltage and current curves obtained with the ULM and a time step of 1 µs: Figures 18 and 19.

Voltage			Current		
Phases	**Model: Δt**	**NRMSD**	**Phases**	**Model: Δt**	**NRMSD**
1 (Figure 18)	PFLE 0.1 µs	0.004	1 (Figure 19)	PFLE 0.1 µs	2×10^{-4}
	PFLE 1 µs	0.003		PFLE 1 µs	3×10^{-4}
	PFLE 2 µs	0.003		PFLE 2 µs	2×10^{-4}
	PFLE 4 µs	0.005		PFLE 4 µs	1×10^{-4}
2 and 3 (Figure 18)	2	0.005	2 and 3 (Figure 19)	PFLE 0.1 µs	42×10^{-4}
	PFLE 1 µs	0.003		PFLE 1 µs	1×10^{-4}
	PFLE 2 µs	0.003		PFLE 2 µs	2×10^{-4}
	PFLE 4 µs	0.005		PFLE 4 µs	4×10^{-4}

Table 4. NRMSD of the voltage and current curves obtained with the PFLE with respect to the voltage and current curves obtained with the ULM and a time step of 1 µs: Figures 22 and 23.

Voltage			Current		
Phases	**Model**	**NRMSD**	**Phases**	**Model**	**NRMSD**
1 (Figure 22)	PFLE 0.1 µs	0.004	1 (Figure 23)	PFLE 0.1 µs	3×10^{-4}
	PFLE 1 µs	0.003		PFLE 1 µs	3×10^{-4}
	PFLE 2 µs	0.003		PFLE 2 µs	1×10^{-4}
	PFLE 4 µs	0.005		PFLE 4 µs	1×10^{-4}
2 and 3 (Figure 22)	PFLE 0.1 µs	0.005	2 and 3 (Figure 23)	PFLE 0.1 µs	2×10^{-4}
	PFLE 1 µs	0.003		PFLE 1 µs	2×10^{-4}
	PFLE 2 µs	0.003		PFLE 2 µs	1×10^{-4}
	PFLE 4 µs	0.005		PFLE 4 µs	4×10^{-4}

5. Conclusions

In this paper, we propose an alternative frequency-dependent transmission line (TL) model based on the folded line equivalent (FLE) line model to represent three-phase TLs. The proposed approach uses a circuit representation of Clarke's matrix to transform parameters from the phase domain to the mode domain. Then, instead of using the transformation matrix proposed in [8], we use a new transformation matrix to transform parameters from the mode domain to the FLE domain. The proposed matrix allows the proposed model to be implemented in simulation software using ideal transformers. The open-circuit and short-circuit contributions of the proposed approach are represented in simulation software using Norton equivalent circuits. We implement the proposed approach in MatLab's Simulink multidomain simulation software.

Traditional TL models based on the method of characteristics can only run in simulations where the time step is equal to or less than the propagation delay of the shortest TL in the network. The main advantage of the proposed approach is that it can run on simulations where the step size is greater than the propagation time of the TL without compromising accuracy. Figure 14 through Figure 23 show good agreement between the results obtained with the ULM and the PFLE. Furthermore, they show that the PFLE provides accurate results even when the time step is four times greater than the propagation delay of the TL. Tables 1–4 show that the NRMSD of the results obtained by the PFLE, when compared to the results obtained by the ULM with a time step of 1/10 of the propagation delay of the TL, is less than 0.005. These results prove that the proposed model outputs accurate results in simulations where the time step is 10%, 100%, 200%, and 400% of the propagation time of the TL.

Author Contributions: Conceptualization, J.S.L.C., S.K., L.T., P.T.C. and J.P.F.; methodology, J.S.L.C. and L.T.; software, J.S.L.C. and L.T.; validation, J.S.L.C. and L.T.; formal analysis, J.S.L.C., L.T. and P.T.C.; investigation, J.S.L.C. and L.T.; writing—original draft preparation, J.S.L.C., L.T. and P.T.C.; visualization, J.S.L.C. and L.T.; supervision, P.T.C., S.K. and J.P.F.; project administration, S.K. and J.P.F.; funding, S.K. All authors have read and agreed to the published version of the manuscript.

Funding: This work was funded by the Coordenação de Aperfeiçoamento de Pessoal de Nível Superior—Finance code 001, the São Paulo Research Foundation grant: 2021/06157-5, and the Centro de Pesquisa e Desenvolvimento em Telecomunicações.

Institutional Review Board Statement: Not applicable.

Informed Consent Statement: Not applicable.

Data Availability Statement: Not applicable.

Conflicts of Interest: The authors declare no conflict of interest.

Abbreviations

The following abbreviations are used in this manuscript:

TL	Transmission line
ATP-EMTP	Alternative Transient Program-Electromagnetic Transients Program
ULM	Universal Line Model
PSCAD	Power Systems Computer Aided Design
EMRP-RV	Electromagnetic Transients Program-Restructured Version
FLE	Folded Line Equivalent
VF	Vector Fitting
p.u.l.	per unit length
FMP	Fast Modal Perturbation
PFLE	Proposed Folded Line Equivalent

References

1. Marti, J.R. Accurate Modeling of Frequency-Dependent Transmission Lines in Electromagnetic Transient Simulations. *IEEE Power Eng. Rev.* **1982**, *2*, 29–30. [CrossRef]
2. Laurent Dubé European EMTP-ATP Users Group e.V. Users Guide to Models in ATP. April 1999. Available online: https://pdfcoffee.com/users-guide-to-models-in-atp-acknowledgments-pdf-free.html (accessed on 30 January 2022).
3. Morched, A.S.; Gustavsen, B.; Tartibi, M. A universal model for accurate calculation of electromagnetic transients on overhead lines and underground cables. *IEEE Trans. Power Deliv.* **1999**, *14*, 1032–1037. [CrossRef]
4. Manitoba HVDC Research Centre Inc. *PSCAD-EMTDC Version 4.5 The Professional's Tool for Electromagnetic Transients Simulation*; Manitoba HVDC Research Centre, Inc.: Winnipeg, MB, Canada, 2008.
5. EMTP-RV. 2021. Available online: http://emtp.com/ (accessed on 1 February 2022).
6. Dommel, H.W. Digital Computer Solution of Electromagnetic Transients in Single-and Multiphase Networks. *IEEE Trans. Power Appar. Syst.* **1969**, *PAS-88*, 388–399. [CrossRef]
7. De Silva, H.M.J.; Kariyawasam, K.K.M.A.; Gole, A.M.; Nordstrom, J.E. Accurate time domain simulation of frequency dependent transmission line models for large time steps. In Proceedings of the International Conference on Power Systems Transients (IPST), Vancouver, BC, Canada, 18–20 July 2013.
8. Gustavsen, B.; Semlyen, A. Admittance-Based Modeling of Transmission Lines by a Folded Line Equivalent. *IEEE Trans. Power Deliv.* **2009**, *24*, 231–239. [CrossRef]
9. Gustavsen, B.; Semlyen, A. Rational approximation of frequency domain responses by vector fitting. *IEEE Trans. Power Deliv.* **1999**, *14*, 1052–1061. [CrossRef]
10. Gustavsen, B. Improving the pole relocating properties of vector fitting. *IEEE Trans. Power Deliv.* **2006**, *21*, 1587–1592. [CrossRef]
11. Simscape Electrical User's Guide (Specialized Power Systems). Hydro-Quebec and Math Works. 2022. Available online: https://www.mathworks.com/help/physmod/sps/ (accessed on 1 February 2022).
12. Morched, A.S.; Ottevangers, J.H.; Marti, L. Multi-port frequency dependent network equivalents for the EMTP. *IEEE Trans. Power Deliv.* **1993**, *8*, 1402–1412. [CrossRef]
13. Semlyen, A.; Gustavsen, B. Phase-Domain Transmission-Line Modeling With Enforcement of Symmetry Via The Propagated Characteristic Admittance Matrix. *IEEE Trans. Power Deliv.* **2012**, *27*, 626–631. [CrossRef]
14. Gustavsen, B. Validation of frequency-dependent transmission line models. *IEEE Trans. Power Deliv.* **2005**, *20*, 925–933. [CrossRef]

15. Tavares, M.C.; Pissolato, J.; Portela, C.M. New mode domain multiphase transmission line model-transformation matrix modeling. In Proceedings of the POWERCON, International Conference on Power System Technology, Proceedings (Cat. No.98EX151), Beijing, China, 18–21 August 1998; Volume 2, pp. 855–859. [CrossRef]
16. Colqui, J.S.L.; Timaná, L.; Caballero, P.T.; Kurokawa, S.; Filho, J.P. Implementation of modal domain transmission line models in the ATP software. *IEEE Access* **2022**, *10*, 15924–15934. [CrossRef]
17. Gustavsen, B.; De Silva, H.M.J. Inclusion of Rational Models in an Electromagnetic Transients Program: Y-Parameters, Z-Parameters, S-Parameters, Transfer Functions. *IEEE Trans. Power Deliv.* **2013**, *28*, 1164–1174. [CrossRef]
18. Gustavsen, B. Computer code for rational approximation of frequency dependent admittance matrices. *IEEE Trans. Power Deliv.* **2002**, *17*, 1093–1098. [CrossRef]
19. Gustavsen, B. Fast Passivity Enforcement for Pole-Residue Models by Perturbation of Residue Matrix Eigenvalues. *IEEE Trans. Power Deliv.* **2008**, *23*, 2278–2285. [CrossRef]
20. Gustavsen, B. *Matrix Fitting Toolbox (User's Guide and Reference)*; SINTEF Energy Research: Trondheim, Norway, 2009.
21. Gustavsen, B. *User's Guide for Vectfit3.m (Fast Relaxed Vector Fitting)*; SINTEF Energy Research: Trondheim, Norway, 2008.
22. Boyd, S.; Chua, L.O. On the passivity criterion for LTI n-ports. *Circuit Theory Appl.* **1982**, *10*, 323–333. [CrossRef]